Magnetoelastically induced vibronic bound state in the spin-ice pyrochlore $Ho_2Ti_2O_7$

J. Gaudet,[1] A. M. Hallas,[1] C. R. C. Buhariwalla,[1] G. Sala,[1,2] M. B. Stone,[2] M. Tachibana,[3] K. Baroudi,[4] R. J. Cava,[4,5] and B. D. Gaulin[1,6,7]

[1]*Department of Physics and Astronomy, McMaster University, Hamilton, ON, Canada L8S 4M1*
[2]*Neutron Scattering Division, Oak Ridge National Laboratory, Oak Ridge, Tennessee 37831, USA*
[3]*National Institute for Materials Science, 1-1 Namiki, Tsukuba 305-0044, Ibaraki, Japan*
[4]*Department of Chemistry, Princeton University, Princeton, New Jersey 08544, USA*
[5]*Princeton Materials Institute, Princeton University, Princeton, New Jersey 08544, USA*
[6]*Canadian Institute for Advanced Research, Toronto, Canada M5G 1M1*
[7]*Brockhouse Institute for Materials Research, Hamilton, ON, Canada L8S 4M1*

(Received 8 May 2018; published 19 July 2018)

The single-ion physics of $Ho_2Ti_2O_7$ is well understood to produce strong Ising anisotropy, which is an essential ingredient to its low-temperature spin-ice state. We present inelastic neutron scattering measurements on $Ho_2Ti_2O_7$ that reveal a clear inconsistency with its established single-ion Hamiltonian. Specifically, we show that a crystal-field doublet near 60 meV is split by approximately 3 meV. Furthermore, this crystal-field splitting is not isolated to $Ho_2Ti_2O_7$ but can also be found in its chemical pressure analogs $Ho_2Ge_2O_7$ and $Ho_2Sn_2O_7$. We demonstrate that the origin of this effect is a vibronic bound state, resulting from the entanglement of a phonon and crystal-field excitation. We derive the microscopic Hamiltonian that describes the magnetoelastic coupling and provides a quantitative description of the inelastic neutron spectra.

DOI: 10.1103/PhysRevB.98.014419

I. INTRODUCTION

The pyrochlore oxide $Ho_2Ti_2O_7$ is a quintessential dipolar spin-ice material [1]. In this system, the Ho^{3+} moments sit on the vertices of a corner-sharing tetrahedral network. Each Ho^{3+} moment possesses strong local Ising anisotropy such that each spin is constrained to point either towards ("in") or away from ("out") the center of their respective tetrahedra [2,3]. At low temperatures, below $\theta_{CW} = 2$ K, the Ho^{3+} moments adopt a two-in/two-out arrangement, a spin structure that exactly maps onto the proton configuration in water ice [2,4]. In addition to moments with local Ising anisotropy decorating the pyrochlore lattice, the other key ingredient for the dipolar spin-ice state is an effective ferromagnetic coupling between the Ho^{3+} moments, which originates from long-range dipolar interactions [5]. A decade after the initial discovery of the dipolar spin-ice state in $Ho_2Ti_2O_7$ [2], a host of studies revealed that the elementary spin excitations in this state are emergent magnetic monopoles [6–11].

Although Ising anisotropy is a key ingredient to the spin-ice state, it has been the subject of relatively few investigations [3,12,13]. Naturally, most studies on $Ho_2Ti_2O_7$ have focused on the collective spin behavior within the ice state. Here, taking advantage of recent advances in the instrumentation of time-of-flight neutron spectroscopy, we take a closer and more comprehensive look at the crystal-electric-field (CEF) scheme of $Ho_2Ti_2O_7$ and two of its sister spin-ice materials $Ho_2Sn_2O_7$ [14,15] and $Ho_2Ge_2O_7$ [16,17]. In doing so, we observe a splitting of a high-energy CEF excitation, a feature that could not be observed in previous neutron scattering works due to their lower-energy resolution. We show that this split excitation cannot be accounted for by either a pure CEF excitation or by a pure phonon excitation. We conclude that its origin is a magnetoelastic coupling induced vibronic bound state, a hybridized excitation resulting from the entanglement of a phonon and a crystal-field excitation.

The vibronic bound state is a quantum phenomenon that is challenging to unambiguously identify because it requires a detailed independent knowledge of a material's phonon dispersion and CEF scheme [18]. Consequently, there have been few definitive examples of materials with this phenomenology and these have generally been limited to materials with uncomplicated CEF spectra. For example, the landmark observation of a vibronic bound state in $CeAl_2$ [19,20] was aided by the fact that only a single excited CEF level is expected in this material. Another notable example is the high-T_C superconductor $NdBa_2Cu_3O_{7-\delta}$, where isotopic substitution of oxygen was used to shift the phonon energy, thereby altering the nature of the bound state [21]. Our work expands the notion of vibronic bound states to the pyrochlore magnet $Ho_2Ti_2O_7$, a material with a considerably more complex CEF scheme. We propose that in addition to being prototypical spin-ice materials, $Ho_2Ti_2O_7$ and its sister holmium pyrochlores are also quintessential examples of materials that exhibit a vibronic bound state.

II. RESULTS

In the holmium pyrochlores, the local spin anisotropy depends only on the composition of the CEF ground state, which in turn depends on the symmetry and strength of the CEF at the Ho^{3+} site. In the case of D_{3d} point-group symmetry, which is appropriate for the rare-earth site in the pyrochlore lattice, the CEF Hamiltonian can be expressed as follows [22–25]:

$$\begin{aligned}\mathcal{H}_{\mathrm{CEF}} = {} & A_2^0\alpha_J\langle r^2\rangle\hat{O}_2^0 + A_4^0\beta_J\langle r^4\rangle\hat{O}_4^0 \\ & + A_4^3\beta_J\langle r^4\rangle\hat{O}_4^3 + A_6^0\gamma_J\langle r^6\rangle\hat{O}_6^0 \\ & + A_6^3\gamma_J\langle r^6\rangle\hat{O}_6^3 + A_6^6\gamma_J\langle r^6\rangle\hat{O}_6^6, \end{aligned} \quad (1)$$

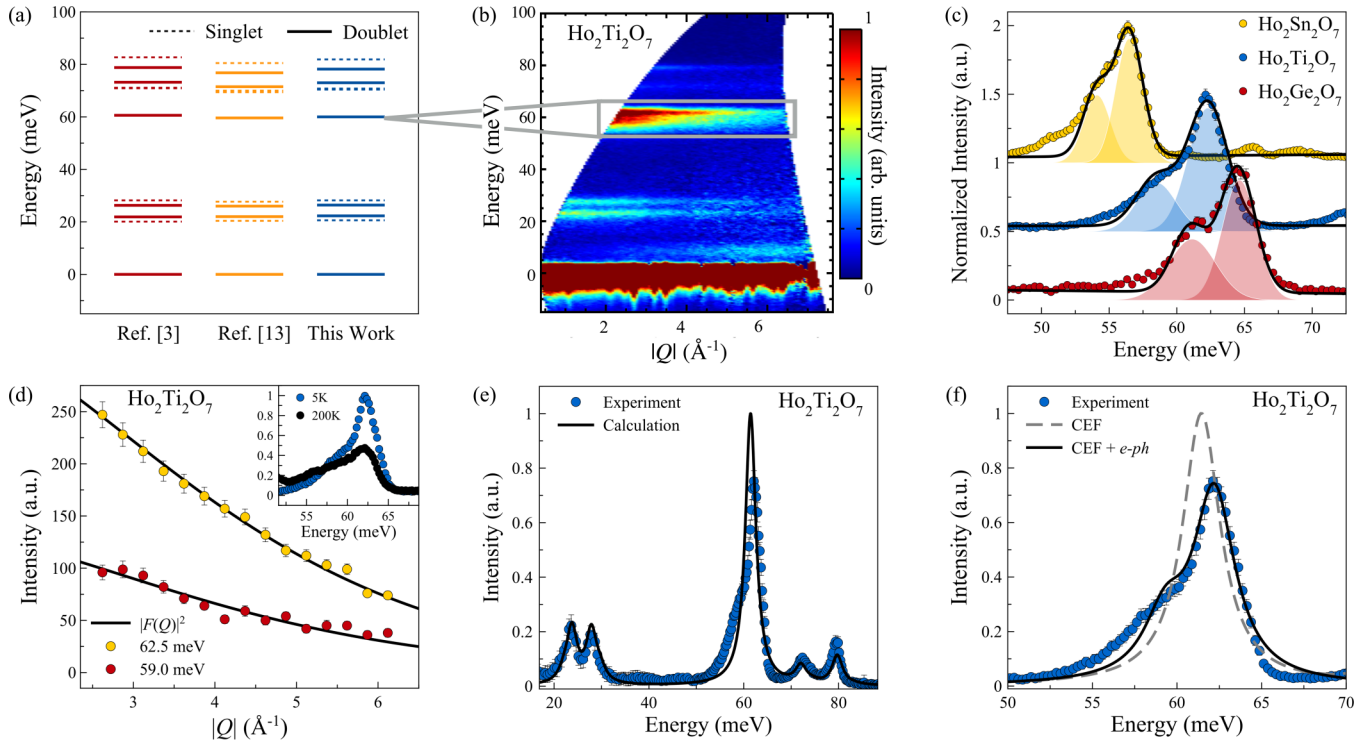

FIG. 1. (a) The CEF energy scheme for $Ho_2Ti_2O_7$ deduced by Rosenkranz *et al.* [3], Ruminy *et al.* [13], and our current work. This scheme was determined via inelastic neutron scattering measurements, such as the one shown in (b), a spectrum that was collected with $E_i = 150$ meV at $T = 5$ K. (c) Integrated scattering from 3 to 4 Å^{-1} reveals a splitting of the CEF level near 60 meV in each of $Ho_2Ge_2O_7$, $Ho_2Ti_2O_7$, and $Ho_2Sn_2O_7$. (d) Both of the excitations near 60 meV follow the magnetic form factor for Ho^{3+}, where the intensities were extracted by fitting to the sum of two Gaussians, as depicted in (c). The temperature dependence is also consistent with a magnetic origin, as shown in the inset. (e) Our refined CEF Hamiltonian for $Ho_2Ti_2O_7$ gives a good description of the experimental data, but does not capture the splitting near 60 meV. (f) The splitting can be modeled by including a magnetoelastic term in our Hamiltonian, which describes the hybridization of the CEF level with a phonon.

where the $\hat{O}_m^n$ are Stevens operators [26]. The α_J, β_J, and γ_J are reduced matrix elements calculated in Ref. [26]. The terms $\langle r^n \rangle$ are the expected value of the distance between the nucleus and the $4f$ electron shell taken to the nth power, and are tabulated in Ref. [27]. According to the symmetry of the CEF Hamiltonian, the $2J + 1 = 17$ states of the spin-orbit ground state are split into six doublets and five singlets. The energy configuration and composition of these CEF states are controlled by the CEF parameters A_n^m, which can be estimated from point-charge calculations [22] or experimentally determined by inelastic neutron spectroscopy [28].

The single-ion properties of $Ho_2Ti_2O_7$ have been previously studied with inelastic neutron scattering by Rosenkranz *et al.* [3] and Ruminy *et al.* [13]. In Fig. 1(a), we reproduce the CEF energy scheme of $Ho_2Ti_2O_7$ based on these earlier works. In both cases, the ground state is a well-isolated non-Kramers doublet. The first set of excited crystal-field levels, which are located between 20 and 30 meV, is made up of two singlets and two doublets, followed by an isolated doublet at 60 meV and, finally, two doublets and three singlets between 70 and 90 meV. The four closely spaced doublet/singlet pairs are the products of a distorted cubic oxygen environment, where in a precisely cubic environment, these would form four triplets [29]. The most important result for the low-temperature magnetism is that the ground-state doublet consists of two states with dominant $|m_J = \pm 8\rangle$, resulting in a strong local Ising anisotropy.

We have carried out inelastic neutron scattering measurements to investigate the CEF schemes of three holmium pyrochlores: $Ho_2Ge_2O_7$, $Ho_2Ti_2O_7$, and $Ho_2Sn_2O_7$. In each of these three materials the magnetism originates from Ho^{3+} and the variation from nonmagnetic Ge to Ti to Sn primarily modifies the cubic lattice parameter. $Ho_2Ge_2O_7$ and $Ho_2Sn_2O_7$ can be considered as positive and negative chemical pressure analogs of $Ho_2Ti_2O_7$, respectively. The inelastic neutron scattering measurements were performed using a next-generation chopper spectrometer, SEQUOIA, at the Spallation Neutron Source at Oak Ridge National Laboratory [30]. The full inelastic spectra for each of these three materials can be found in the Appendices as well as further experimental details.

We begin by considering the $E_i = 150$ meV spectra for $Ho_2Ti_2O_7$, which is shown in Fig. 1(b). This data set was collected at $T = 5$ K, which is well below the threshold for thermally populating excited crystal-field states. Thus, at this temperature, all CEF excitations must originate from the ground state. A handful of CEF excitations (at approximately 22, 26, 60, 71, and 78 meV) can be immediately identified based on their lack of dispersion and intensity that decreases as a function of $|\mathbf{Q}|$. By comparing Figs. 1(a) and 1(b), we see that the energies of these excitations are in good agreement with the predicted energy schemes of the previous CEF studies on $Ho_2Ti_2O_7$ [3,13]. However, a closer examination of the scattering spectra near 60 meV reveals a striking inconsistency:

TABLE I. Tabulated results of the CEF analysis for $Ho_2Ge_2O_7$, $Ho_2Ti_2O_7$, and $Ho_2Sn_2O_7$ including the CEF parameters A_m^n (in meV), the Ising component of the local g tensor g_z, and the effective moment of the ground-state doublet $\mu_{\rm CEF}$ (in μ_B). We then give the calculated and experimental values of the splitting energy ΔE (in meV), and intensity ratio $I^{\rm ratio}$ of the split CEF level at 60 meV. The final two columns give the refined magnetoelastic constant g_0 and phonon energy $\hbar\omega_0$ (in meV).

	A_2^0	A_4^0	A_4^3	A_6^0	A_6^3	A_6^6	g_z	$\mu_{\rm CEF}$	$\Delta E_{\rm expt}$	$\Delta E_{\rm calc}$	$I^{\rm ratio}_{\rm expt}$	$I^{\rm ratio}_{\rm calc}$	g_0	$\hbar\omega_0$
$Ho_2Ge_2O_7$	64.9	27.3	185	1.05	−16.9	24.0	19.4	9.7	3.1(2)	2.8	2.5(1)	2.5	0.04(1)	65(1)
$Ho_2Ti_2O_7$	50.3	26.1	185	1.05	−15.6	20.0	19.6	9.8	3.5(2)	3.6	2.5(1)	2.4	0.04(1)	61(1)
$Ho_2Sn_2O_7$	59.7	22.7	191	0.93	−14.7	19.0	19.6	9.8	2.4(2)	2.6	2.1(1)	2.1	0.04(1)	55(1)

there are two distinct excitations near 60 meV in our new experimental data instead of the single well isolated CEF excitation predicted by the Hamiltonians of both Rosenkranz *et al.* [3] and Ruminy *et al.* [13]. This can be better appreciated by performing an integration over the energy interval in question, which is shown in Fig. 1(c). A similar structure is observed for the equivalent excitations in $Ho_2Ge_2O_7$ and $Ho_2Sn_2O_7$, which occur at respectively slightly higher- and lower-energy transfers. In each case, the lower-energy excitation has less than half the intensity of the higher-energy one. In the paragraphs that follow, we will address the plausible origins for these two excitations and ultimately show that their origin is a magnetoelastic coupling induced vibronic bound state.

III. ANALYSIS AND DISCUSSION

We will first demonstrate that a pure phonon excitation is not the origin of either of the excitations near 60 meV. This can be verified by analyzing the $|\mathbf{Q}|$ dependence of their scattered intensity, which is presented in Fig. 1(d) for $Ho_2Ti_2O_7$. The intensities of the two excitations were extracted by taking integrations of the data set shown in Fig. 1(b) in 0.2-Å^{-1} intervals, which were then fit to the sum of two Gaussian functions. Examples of such fits for each of the three holmium pyrochlores are given in Fig. 1(c). In all three samples, the intensities of both excitations are observed to decrease monotonically with $|\mathbf{Q}|$, a behavior that is unmistakably inconsistent with the $\mathbf{Q}^2$ dependence expected for a pure phonon excitation [31]. Instead, as shown in Fig. 1(d), the $|\mathbf{Q}|$ dependence of both excitations agrees well with the magnetic form factor for Ho^{3+}, which is the expected behavior for a CEF excitation. Furthermore, as seen in the inset of Fig. 1(d), the intensities of both excitations decrease when the temperature is raised from 5 to 200 K, a temperature dependence that is also inconsistent with the behavior of a phonon excitation.

Given that the 60-meV excitations have intensities that follow the magnetic form factor for Ho^{3+}, we next considered the possibility that they are both pure CEF excitations. Thus, we attempted to refine a new CEF Hamiltonian for $Ho_2Ti_2O_7$ that includes two or more CEF levels around 60 meV. We followed the same method used in Refs. [3,32], which consists of varying the set of CEF parameters, A_m^n in Eq. (1), until a minimum value of χ^2 is reached between the computed and experimental CEF spectrum. However, this search did not yield any satisfactory result; over an extensive range of parameter space all solutions with multiple transitions near 60 meV contained glaring inconsistencies with other features in the experimental spectrum. Furthermore, having two CEF transitions near 60 meV for $Ho_2Ti_2O_7$ is also inconsistent with point-charge calculations [28,33]. Starting from a robust, highly constrained determination of the CEF Hamiltonian for the erbium pyrochlore $Er_2Ti_2O_7$, we apply a scaling procedure to approximate the CEF Hamiltonians of other titanate pyrochlores [32]. Using this scaling argument, the calculated CEF scheme for $Ho_2Ti_2O_7$, aside from containing only a single isolated excitation near 60 meV, is in excellent qualitative agreement with our experimental data and the previous reports by Rosenkranz *et al.* [3] and Ruminy *et al.* [13]. Moreover, when this scaling procedure is performed in reverse, starting from a CEF Hamiltonian for $Ho_2Ti_2O_7$ that contains two excitations near 60 meV, the scaling gives results which are wholly inconsistent with the known CEF spectra for $Tb_2Ti_2O_7$ [13,34], $Er_2Ti_2O_7$ [32], and $Yb_2Ti_2O_7$ [35]. Thus, we conclude that the two excitations near 60 meV cannot be pure CEF excitations and must originate from the degeneracy breaking of the CEF doublet.

Putting aside the origin of the split doublet for a moment, we will first describe the results of our conventional CEF analysis on the three holmium pyrochlores. For this analysis, we disregarded the splitting of the 60-meV doublet and assigned its energy as the average value, 60.8 meV for $Ho_2Ti_2O_7$, and assigned its intensity as the total value for both excitations. The CEF Hamiltonians obtained for all three holmium pyrochlores are given in Table I. The calculated energies and intensities for $Ho_2Ge_2O_7$, $Ho_2Ti_2O_7$, and $Ho_2Sn_2O_7$ are tabulated in the Appendices and result in χ^2 values of 1.5, 1.0, and 1.1, respectively. In Fig. 1(a), we schematically present the energy scheme for $Ho_2Ti_2O_7$ based on our parametrization side by side with those of the previous studies [3,13], showing that they are entirely consistent with one another. The computed inelastic neutron scattering spectra for $Ho_2Ti_2O_7$ at $T = 5$ K is shown in Fig. 1(e), and provides an excellent description of the experimental data aside from the obvious discrepancy near 60 meV. The ground-state CEF doublet is, as expected, highly anisotropic. The component of the local g tensor perpendicular to the Ising axis is strictly zero. In fact, this is provided by symmetry for a non-Kramers doublet since, under time reversal, J_z transforms like a magnetic dipole while J_x, J_y transform like an electric quadrupole [36]. The component parallel to the local Ising axis (g_z) as well as the effective moment of the CEF ground state doublet are listed in Table I. Neither of these quantities are observed to significantly vary with chemical pressure. Thus, as it relates to their spin-ice physics, the holmium pyrochlores are effectively identical in terms of their CEF properties.

We return now to the degeneracy breaking of the CEF doublet near 60 meV. One possibility is that a symmetry-reducing structural distortion could be responsible for lifting the degeneracy of this doublet. However, highly sensitive

neutron Larmor diffraction measurements have shown that no such transition occurs in $Ho_2Ti_2O_7$ down to 0.5 K [37]. Exchange interactions could also produce a degeneracy breaking, but the energy scale of the exchange interactions in rare-earth pyrochlores is of order 1 meV [8], whereas the splitting of the CEF doublet is observed to persist up to at least 200 K ($k_BT = 17$ meV), as shown in the inset of Fig. 1(d). A final possible origin for the CEF splitting is an electron-phonon or magnetoelastic coupling, and here we have finally arrived at an explanation which, as we now show, is fully compatible with our experimental results.

A magnetoelastic interaction can be modeled by introducing a linear coupling between the phonon displacements of the system and the quadrupolar operator of the Ho^{3+} ion. Including the noninteracting phonon coupling, the system can be described by the following Hamiltonian [19,20]:

$$\mathcal{H}_{\text{tot}} = \mathcal{H}_{\text{CEF}} + \sum_{\mu} \hbar\omega_{\mu}\left(\hat{a}_{\mu}^{\dagger}\hat{a}_{\mu} + \frac{1}{2}\right) - \sum_{\mu,i} g_{\mu}\hat{U}_{\mu}\hat{O}_i, \quad (2)$$

where $\hat{U}_{\mu} = (\hat{a}_{\mu} + \hat{a}_{\mu}^{\dagger})$ is the phonon displacement operator. The operators $\hat{a}_{\mu}$ and $\hat{a}_{\mu}^{\dagger}$ correspond to the annihilation and creation of a phonon with displacement μ and energy $\hbar\omega_{\mu}$. The magnetoelastic constant is given by g_{μ}, while $\hat{O}_i$ corresponds to quadrupolar operators that can be written in terms of total angular momentum operators. For the D_{3d} point-group symmetry, there are five quadrupolar operators with three different symmetries: $\hat{O}_1 = 3J_z^2 - J(J+1)$, $\hat{O}_{2,3} = J_x^2 - J_y^2$, $J_xJ_y + J_yJ_x$, and $\hat{O}_{4,5} = J_xJ_z + J_zJ_x$, $J_yJ_z + J_zJ_y$. Magnetoelastic coupling between two CEF states is only allowed if the symmetry of the quadrupolar operator and the phonon eigenvector are identical [38]. The symmetry of the phonon displacements in $Ho_2Ti_2O_7$ was characterized in Ref. [39] and, thus, symmetry analysis can be used to predict which CEF states are candidates for magnetoelastic coupling. Only the CEF states at 26, 60, and 78 meV have quadrupolar and displacement operators of the correct symmetry to couple with the ground state [40]. Furthermore, we find that the matrix element involving the state at 60 meV is an order of magnitude larger than the state at 26 meV and three orders of magnitude larger than the state at 78 meV. This provides a natural explanation for why we only observe a splitting of the 60-meV CEF state.

In order to quantify the magnetoelastic coupling, we extracted the eigenvectors associated with the ground state (v_1, v_2) and the 60-meV excited state (v_3, v_4) obtained from our CEF analysis. The noninteracting phonon contribution was approximated by a single phonon of energy $\hbar\omega_0$. Then, the Hamiltonian shown in Eq. (2) was diagonalized using the following states: $|v_{cef}, v_{ph}\rangle = |v_1,0\rangle, |v_2,0\rangle, |v_1,\hbar\omega_0\rangle, |v_2,\hbar\omega_0\rangle, |v_3,0\rangle, |v_4,0\rangle$. A splitting of the 60-meV CEF level is observed whenever the magnetoelastic constant g_0 is nonzero and the energy of the phonon $\hbar\omega_0$ is close to that of the CEF level. To determine the precise values of g_0 and $\hbar\omega_0$, we performed a least-squares refinement of the energy difference (ΔE) and the intensity ratio (I^{ratio}) of the split CEF level. The refined values of g_0 and $\hbar\omega_0$ are tabulated in Table I, along with a comparison of the experimental and calculated values of ΔE and I^{ratio}. The resulting CEF spectra for $Ho_2Ti_2O_7$ are presented in Fig. 1(f), showing good agreement with the measured data. In each of the three holmium pyrochlores, the splitting does not produce two peaks of equal intensity, but rather the higher-energy excitation is roughly twice the intensity of the lower-energy excitation. This originates from the fact that the phonon involved in the coupling is located at slightly higher energy than the CEF excitation. The phonon involved in this coupling corresponds to an oxygen displacement [39], which may favor magnetoelastic coupling because the oxygen ions provide the dominant contribution to the CEF. The composition of the eigenstates for the split CEF levels, which are given in the Appendices, consists of a linear combination of a pure CEF excitation ($|v_3,0\rangle, |v_4,0\rangle$) and a pure phonon excitation ($|v_1,\hbar\omega_0\rangle, |v_2,\hbar\omega_0\rangle$).

IV. CONCLUSION

We have demonstrated the existence of strong magnetoelastic coupling in the holmium pyrochlores. This coupling is a quantum phenomena that can be termed a vibronic bound state, the coherent propagation of a bound CEF and a phonon excitation. This effect is analogous to the exciton excitation observed in semiconductors where an electron and a hole particle are bound together. Vibronic bound states are rare [18] and have been most frequently observed in cerium-based intermetallics, such as $CeAl_2$ and $CeCuAl_3$ [19,41–43]. Within the pyrochlore family of materials, magnetoelastic coupling has been argued as relevant in the spin-liquid behavior of $Tb_2Ti_2O_7$, where vibronic excitations were also observed [13,44,45]. However, in the case of $Tb_2Ti_2O_7$, where the coupling occurs at 1 meV, a quantitative description has not yet been achieved due to the complex influence of exchange interactions. Magnetoelastic coupling has also been investigated in the context of spin ice, where the monopole dynamics has been shown to depend on the spin-lattice interaction [40,46,47]. Considering the body of work including our new findings, it is clear that magnetoelastic coupling is an important interaction in the rare-earth pyrochlores and that it will play a major role in the discovery of new quantum phenomena.

ACKNOWLEDGMENTS

This research at ORNL's Spallation Neutron Source was sponsored by the Scientific User Facilities Division, Office of Basic Energy Sciences, US Department of Energy. This work was supported by the Natural Sciences and Engineering Research Council of Canada. The sample growth at Princeton University was supported by the US Department of Energy, Basic Energy Sciences, through the IQM at Johns Hopkins University, Grant No. DE-FG02-98-ER46544.

APPENDIX A: EXPERIMENTAL METHODS

Powder samples of $Ho_2Ti_2O_7$, $Ho_2Sn_2O_7$, and $Lu_2Ti_2O_7$ of approximately 10 g each were prepared by conventional solid-state synthesis. The 1.8 g sample of $Ho_2Ge_2O_7$ was synthesized using high-pressure techniques following the same protocol as Ref. [48]. The samples of $Ho_2Ti_2O_7$ and $Ho_2Sn_2O_7$ were loaded in helium atmosphere between flat aluminum plates and sealed with indium. The samples of $Ho_2Ge_2O_7$ and $Lu_2Ti_2O_7$ were sealed in the same manner, but in an annular

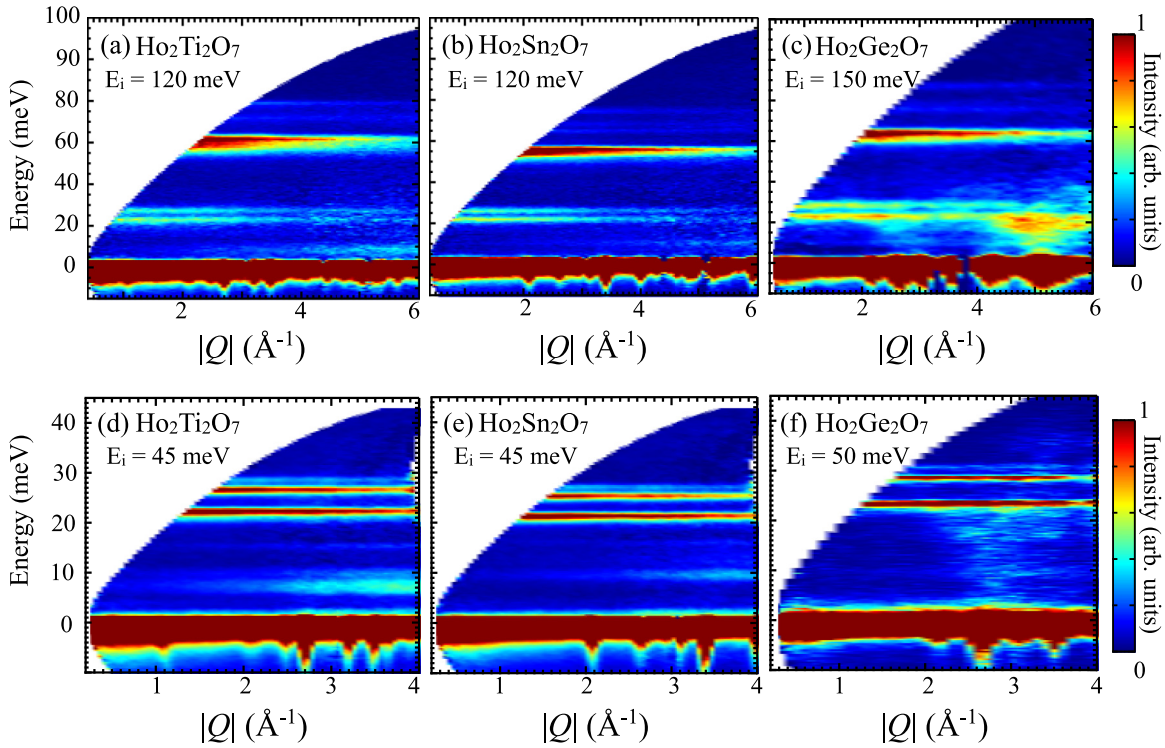

FIG. 2. Neutron scattering spectra obtained for an incident energy of 120 or 150 meV for (a) $Ho_2Ti_2O_7$, (b) $Ho_2Sn_2O_7$, and (c) $Ho_2Ge_2O_7$ and for an incident energy of 45 or 50 meV for (e) $Ho_2Ti_2O_7$, (f) $Ho_2Sn_2O_7$, and (g) $Ho_2Ge_2O_7$. These data sets were collected at 5 K for $Ho_2Ti_2O_7$ and $Ho_2Sn_2O_7$ and 2 K for $Ho_2Ge_2O_7$.

aluminum can. Inelastic neutron scattering measurements were performed on all three holmium pyrochlores as well as the nonmagnetic $Lu_2Ti_2O_7$ with the time-of-flight spectrometer SEQUOIA at the Spallation Neutron Source at Oak Ridge National Laboratory [30]. The measurements for $Ho_2Ti_2O_7$, $Ho_2Sn_2O_7$, and $Lu_2Ti_2O_7$ were performed in a closed-cycle refrigerator, giving a base temperature of 5 K, while $Ho_2Ge_2O_7$ was measured in an orange ILL liquid-helium cryostat, giving a base temperature of 2 K. Data sets were collected for each sample with a lower incident energy (either 45 or 50 meV) and a higher incident energy (120 or 150 meV). The fine Fermi chopper was used to give the maximum energy resolution for each incident energy, approximately 1 meV for the lower-energy data sets and 3 meV for the higher-energy data sets at the elastic line. An empty flat plate was also measured under an identical configuration, and was subtracted from the data. The data were reduced using MANTID [49] and analyzed with DAVE [50].

APPENDIX B: DETERMINATION OF THE CEF HAMILTONIANS

Inelastic neutron scattering measurements with $E_i = 120$ or 150 meV [Figs. 2(a)–2(c)] and $E_i = 45$ or 50 meV [Figs. 2(d)–2(f)] were performed in order to determine the CEF Hamiltonians of $Ho_2Ti_2O_7$, $Ho_2Sn_2O_7$, and $Ho_2Ge_2O_7$. As can be seen by comparing Figs. 2(a) and 2(d) with Figs. 2(b) and 2(e) and Figs. 2(c) and 2(f), the CEF schemes of the three holmium pyrochlores are qualitatively similar. A quantitative analysis of the CEF excitations was achieved by integrating over momentum transfer $|\mathbf{Q}|$ between 4 and 5 Å^{-1} for $E_i = 120$ or 150 meV and between 2 and 3 Å^{-1} for $E_i = 45$ or 50 meV. The resultant integrated intensities are shown for $Ho_2Ti_2O_7$ in Fig. 3. Each CEF transition was fit with a Lorentzian function in order to extract its energy and scattered intensity. The resulting fit for $Ho_2Ti_2O_7$ is shown in Fig. 3. Note that the first excited CEF level is located at 20 meV ($E/k_B = 230$ K) and is thus not thermally populated at 5 K. Therefore, all observed CEF levels correspond to excitations out of the ground state. The CEF transition near 20 meV was clearly resolved in both the low ($E_i = 45$ or 50 meV) and high ($E_i = 120$ or 150 meV) energy spectra and was used to normalize the two data sets. The energy of the CEF transition near 60 meV was taken as the average energy of the split CEF excitation. The observed energies ($E_{\rm obs}$) and scattered intensities ($I_{\rm obs}$) fitted for all three compounds are presented in Table II. The CEF Hamiltonians were refined following the same χ^2 minimization method used in Ref. [32]. The CEF parameters of $Ho_2Ti_2O_7$ obtained in Ref. [3] were used as the starting solution and the χ^2 minimization leads to the refined CEF parameters, A_m^n shown in Table I of the main paper. The calculated CEF transition energies and scattered intensities are given in Table II.

APPENDIX C: PHONON EXCITATIONS IN $Lu_2Ti_2O_7$

The neutron scattering spectra of nonmagnetic $Lu_2Ti_2O_7$ was also measured in order to characterize the phonon spectra. In particular, we expect that the phonon spectrum for $Lu_2Ti_2O_7$ should be almost identical to that of $Ho_2Ti_2O_7$, given their structural similarities and comparable cation masses. The $E_i = 150$ meV spectrum of $Lu_2Ti_2O_7$ is shown in Fig. 4(a). All of the features observed in this spectrum have intensities that

TABLE II. The experimentally observed and calculated values of the energies and neutron scattered intensities of the CEF levels in (a) $Ho_2Ti_2O_7$, (b) $Ho_2Sn_2O_7$, and (c) $Ho_2Ge_2O_7$. Each CEF level is identified as doublet (D) or singlet (S) in the most left column. The calculated values were obtained using the refined CEF parameters found in Table I.

	(a) $Ho_2Ti_2O_7$			
	E_{obs}	E_{calc}	I_{obs}	I_{calc}
D	0	0		
S	20.7(2)	20.6	0.03(2)	0.03
D	22.0(2)	22.3	0.19(5)	0.2
D	26.3(3)	26.4	0.17(5)	0.19
S	28.4(2)	28.2	0.03(2)	0.04
D	58.9(4)	59.9	1	1
S	71.2(4)	70.4	0.05(2)	0.04
S		70.8	0.04(2)	0.02
D		72.3		0.007
D	77.9	78.2	0.12(3)	0.11
S		81.9		0.03
	(b) $Ho_2Sn_2O_7$			
	E_{obs}	E_{calc}	I_{obs}	I_{calc}
D	0	0		
S	20.4(2)	20.3	0.03(2)	0.03
D	21.3(2)	21.6	0.18(5)	0.17
D	25.2(2)	25.1	0.15(4)	0.17
S	27.0(2)	26.9	0.03(2)	0.04
D	53.2(4)	54.3	1	1
S	64.3(4)	63.8	0.07(3)	0.04
S	67.8(4)	67.6	0.06(3)	0.02
D		69.3		0.01
D	73.7	73.9	0.10(3)	0.06
S		76.6		0.001
	(c) $Ho_2Ge_2O_7$			
	E_{obs}	E_{calc}	I_{obs}	I_{calc}
D	0	0		
S	21.9(2)	21.8	0.05(2)	0.05
D	23.4(2)	23.6	0.22(5)	0.27
D	28.5(2)	28.4	0.19(2)	0.26
S	30.7(2)	30.7	0.05(2)	0.05
D	62.7(4)	63.2	1	1
S	75.5(5)	74.7	0.09(3)	0.05
S	79.0(4)	78.7	0.03(2)	0.03
D		81.4		0.007
D	87.0(4)	87.4	0.10(3)	0.06
S		91.0		0.001

increase as a function of momentum transfer $|\mathbf{Q}|$, characteristic of phonon excitations. We performed an integration in $\mathbf{Q}$ between 4 and 5 Å^{-1} and a second integration between 6 and 7 Å^{-1}, the results of which are shown in Fig. 4(b). We can see that $Lu_2Ti_2O_7$ has phonon excitations centered just below 10 meV, multiple bands of phonon from 20 to 50 meV, and, finally, bands of phonon excitations centered around 60 and 75 meV. As mentioned in the main paper, the phonon spectrum of $Ho_2Ti_2O_7$ has been previously characterized using density functional theory and resonant inelastic x-ray scattering. This study showed that the low-energy phonons are dominated by Ho^{3+} and Ti^{4+} displacements and the high-energy phonons are mostly dominated by the displacements of the O^{2-} ions. In particular for the magnetoelastic coupling, the phonon involved in the vibronic bound state of $Ho_2Ti_2O_7$ is centered around 60 meV and known to originate from the displacement of the O^{2-} ions. It is interesting to note that in the oxide pyrochlores, the largest contribution to the CEF comes from the oxygen ions. One can speculate that phonons involving oxygen ions are more effective in coupling with a CEF excitation to induce a vibronic bound state.

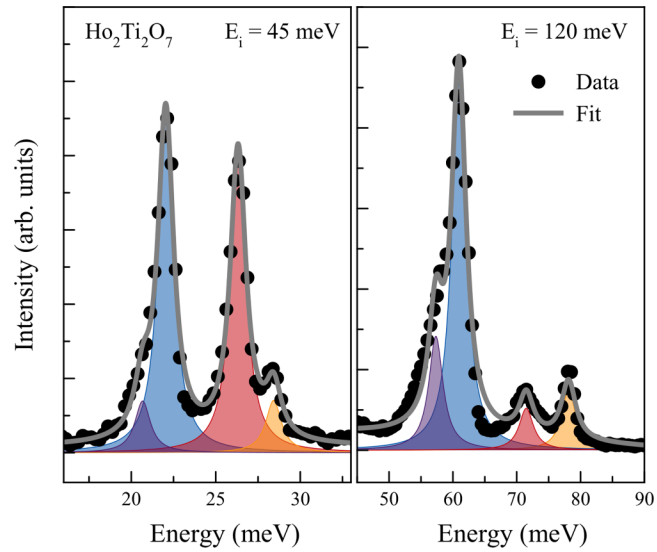

FIG. 3. Integrated scattering spectrum for $Ho_2Ti_2O_7$ at 5 K, obtained by integrating the $E_i = 45$ meV data set from 2 to 3 Å^{-1} and the $E_i = 120$ meV data set from 4 to 5 Å^{-1}. The energies and intensities of the CEF transitions were obtained by fitting to a series of Lorentzian functions, given by the shaded peaks, and their sum is represented by the gray line.

APPENDIX D: DIAGONALIZATION OF THE MAGNETOELASTIC INTERACTION IN THE HOLMIUM PYROCHLORES

The Hamiltonian describing the single-ion properties of the holmium ions in $Ho_2B_2O_7$ is given by

$$\mathcal{H}_{tot} = \mathcal{H}_{CEF} + \sum_{\mu} \hbar\omega_{\mu}\left(\hat{a}^{\dagger}_{\mu}\hat{a}_{\mu} + \frac{1}{2}\right) - \sum_{\mu,i} g_{\mu}\hat{U}_{\mu}\hat{O}_i, \quad \text{(D1)}$$

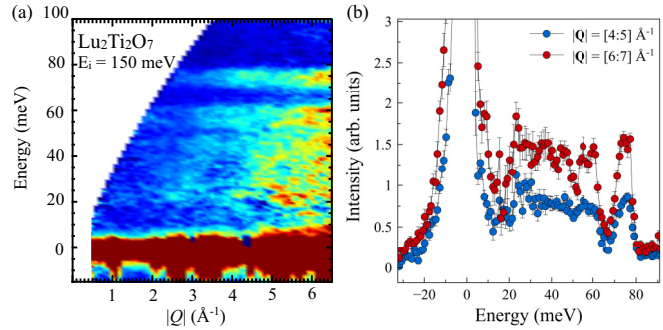

FIG. 4. (a) Inelastic neutron scattering spectra of $Lu_2Ti_2O_7$ measured with $E_i = 150$ meV at 5 K showing the phonon excitation spectrum. (b) Integrations of the scattering spectra between 4 and 5 Å^{-1} and between 6 and 7 Å^{-1} revealing several bands of phonon excitations.

TABLE III. Composition of the vibronic bound state in (a) $Ho_2Ti_2O_7$, (b) $Ho_2Sn_2O_7$, and (c) $Ho_2Ge_2O_7$.

(a) $Ho_2Ti_2O_7$

Energy (meV)	$\|v1,0\rangle$	$\|v2,0\rangle$	$\|v_1,\hbar\omega_0\rangle$	$\|v_2,\hbar\omega_0\rangle$	$\|v3,0\rangle$	$\|v4,0\rangle$
0	1	0	0	0	0	0
0	0	1	0	0	0	0
58.3	0	0	0	−0.425	0.905	0
58.3	0	0	−0.425	0	0	−0.905
61.8	0	0	0	−0.905	−0.425	0
61.8	0	0	0.905	0	0	−0.425

(b) $Ho_2Sn_2O_7$

Energy (meV)	$\|v1,0\rangle$	$\|v2,0\rangle$	$\|v_1,\hbar\omega_0\rangle$	$\|v_2,\hbar\omega_0\rangle$	$\|v3,0\rangle$	$\|v4,0\rangle$
0	1	0	0	0	0	0
0	0	1	0	0	0	0
52.4	0	0	0	−0.529	0.848	0
52.4	0	0	−0.529	0	0	−0.848
55.0	0	0	0	−0.848	−0.529	0
55.0	0	0	0.848	0	0	−0.529

(c) $Ho_2Ge_2O_7$

Energy (meV)	$\|v1,0\rangle$	$\|v2,0\rangle$	$\|v_1,\hbar\omega_0\rangle$	$\|v_2,\hbar\omega_0\rangle$	$\|v3,0\rangle$	$\|v4,0\rangle$
0	1	0	0	0	0	0
0	0	1	0	0	0	0
60.6	0	0	0	−0.494	0.870	0
60.6	0	0	−0.494	0	0	−0.870
63.4	0	0	0	−0.870	−0.494	0
63.4	0	0	0.870	0	0	−0.494

where the first term is the CEF contribution, the second term is the phonon contribution, and the third term is the magnetoelastic coupling. The operators $\hat{a}_\mu$ and $\hat{a}_\mu^\dagger$ correspond to the annihilation and creation of a phonon with displacement μ and energy $\hbar\omega_\mu$ while $\hat{O}_i$ corresponds to quadrupolar operators [example: $\hat{O}_1 = 3J_z^2 - J(J+1)$]. Since we are only interested in the coupling between the CEF ground-state doublet (v_1, v_2) and the CEF excited states near 60 meV (v_3, v_4), we can construct a Hamiltonian that is appropriate only for the v_1, v_2, v_3, v_4 subspace of the CEF term. Furthermore, we assumed the magnetoelastic coupling involves only a single phonon of energy $\hbar\omega_0$. Within such formalism, the Hamiltonian can be simplified as

$$\mathcal{H}_{\text{tot}} = \sum_{i=1,2,3,4} E_i |v_i\rangle\langle v_i| + \hbar\omega_0 \hat{a}_0^\dagger \hat{a}_0 - \sum_i g_0 \hat{U}_0 \hat{O}_i, \quad \text{(D2)}$$

where E_i is the energy of the CEF eigenstate v_i. To diagonalize the magnetoelastic interaction, we use the six following eigenstates: $|v_1,0\rangle$, $|v_2,0\rangle$, $|v_3,0\rangle$, $|v_4,0\rangle$, $|v_1,\hbar\omega_0\rangle$, and $|v_2,\hbar\omega_0\rangle$ where, for example, $|v_1,\hbar\omega_0\rangle$ describes the system with an active phonon of energy $\hbar\omega_0$ and the holmium ion being in its CEF ground state v_1. Assuming a nonzero value for g_0 and the phonon energy $\hbar\omega_0$ that is close to the energy of the CEF states v_3 and v_4, we observe a degeneracy breaking of the v_3 and v_4 CEF states. In order to determine the values of g_0 and $\hbar\omega_0$, we performed a χ^2 refinement of the energy difference (ΔE) and the intensity ratio (I^{ratio}) of the split CEF level. The refined values of ΔE and I^{ratio} are given in Table I. Furthermore, the new eigenstates of the system are given in Table III.

[1] S. T. Bramwell, M. J. Harris, B. C. den Hertog, M. J. P. Gingras, J. S. Gardner, D. F. McMorrow, A. R. Wildes, A. Cornelius, J. D. M. Champion, R. G. Melko, and T. Fennell, Spin Correlations in $Ho_2Ti_2O_7$: A Dipolar Spin Ice System, Phys. Rev. Lett. **87**, 047205 (2001).

[2] M. J. Harris, S. T. Bramwell, D. F. McMorrow, T. H. Zeiske, and K. W. Godfrey, Geometrical Frustration in the Ferromagnetic Pyrochlore $Ho_2Ti_2O_7$, Phys. Rev. Lett. **79**, 2554 (1997).

[3] S. Rosenkranz, A. P. Ramirez, A. Hayashi, R. J. Cava, R. Siddharthan, and B. S. Shastry, Crystal-field interaction in the pyrochlore magnet $Ho_2Ti_2O_7$, J. Appl. Phys. **87**, 5914 (2000).

[4] L. Pauling, The structure and entropy of ice and of other crystals with some randomness of atomic arrangement, J. Am. Chem. Soc. **57**, 2680 (1935).

[5] B. C. den Hertog and M. J. P. Gingras, Dipolar Interactions and Origin of Spin Ice in Ising Pyrochlore Magnets, Phys. Rev. Lett. **84**, 3430 (2000).

[6] C. Castelnovo, R. Moessner, and S. L. Sondhi, Magnetic monopoles in spin ice, Nature (London) **451**, 42 (2008).

[7] L. D. C. Jaubert and P. C. W. Holdsworth, Signature of magnetic monopole and Dirac string dynamics in spin ice, Nat. Phys. **5**, 258 (2009).

[8] T. Fennell, P. P. Deen, A. R. Wildes, K. Schmalzl, D. Prabhakaran, A. T. Boothroyd, R. J. Aldus, D. F. McMorrow, and S. T. Bramwell, Magnetic Coulomb phase in the spin ice $Ho_2Ti_2O_7$, Science **326**, 415 (2009).

[9] D. J. P. Morris, D. A. Tennant, S. A. Grigera, B. Klemke, C. Castelnovo, R. Moessner, C. Czternasty, M. Meissner, K. C. Rule, J.-U. Hoffmann, K. Kiefer, S. Gerischer, D. Slobinsky, and R. S. Perry, Dirac strings and magnetic monopoles in the spin ice $Dy_2Ti_2O_7$, Science **326**, 411 (2009).

[10] S. Ladak, D. E. Read, G. K. Perkins, L. F. Cohen, and W. R. Branford, Direct observation of magnetic monopole defects in an artificial spin-ice system, Nat. Phys. **6**, 359 (2010).

[11] S. R. Giblin, S. T. Bramwell, P. C. W. Holdsworth, D. Prabhakaran, and I. Terry, Creation and measurement of long-lived magnetic monopole currents in spin ice, Nat. Phys. **7**, 252 (2011).

[12] Y. M. Jana and D. Ghosh, Crystal-field studies of magnetic susceptibility, hyperfine, and specific heat properties of a $Ho_2Ti_2O_7$ single crystal, Phys. Rev. B **61**, 9657 (2000).

[13] M. Ruminy, E. Pomjakushina, K. Iida, K. Kamazawa, D. T. Adroja, U. Stuhr, and T. Fennell, Crystal-field parameters of the rare-earth pyrochlores $R_2Ti_2O_7$ (R = Tb, Dy, and Ho), Phys. Rev. B **94**, 024430 (2016).

[14] K. Matsuhira, Y. Hinatsu, K. Tenya, and T. Sakakibara, Low temperature magnetic properties of frustrated pyrochlore ferromagnets $Ho_2Sn_2O_7$ and $Ho_2Ti_2O_7$, J. Phys.: Condens. Matter **12**, L649 (2000).

[15] H. Kadowaki, Y. Ishii, K. Matsuhira, and Y. Hinatsu, Neutron scattering study of dipolar spin ice $Ho_2Sn_2O_7$: Frustrated pyrochlore magnet, Phys. Rev. B **65**, 144421 (2002).

[16] H. D. Zhou, J. G. Cheng, A. M. Hallas, C. R. Wiebe, G. Li, L. Balicas, J. S. Zhou, J. B. Goodenough, J. S. Gardner, and E. S. Choi, Chemical Pressure Effects on Pyrochlore Spin Ice, Phys. Rev. Lett. **108**, 207206 (2012).

[17] A. M. Hallas, J. A. M. Paddison, H. J. Silverstein, A. L. Goodwin, J. R. Stewart, A. R. Wildes, J. G. Cheng, J. S. Zhou, J. B. Goodenough, E. S. Choi, G. Ehlers, J. S. Gardner, C. R. Wiebe, and H. D. Zhou, Statics and dynamics of the highly correlated spin ice $Ho_2Ge_2O_7$, Phys. Rev. B **86**, 134431 (2012).

[18] M. Loewenhaupt and U. Witte, Coupling between electronic and lattice degrees of freedom in $4f$-electron systems investigated by inelastic neutron scattering, J. Phys.: Condens. Matter **15**, S519 (2003).

[19] P. Thalmeier and P. Fulde, Bound State Between a Crystal-Field Excitation and a Phonon in $CeAl_2$, Phys. Rev. Lett. **49**, 1588 (1982).

[20] P. Thalmeier, Theory of the bound state between phonons and a CEF excitation in $CeAl_2$, J. Phys. C: Solid State Phys. **17**, 4153 (1984).

[21] E. T. Heyen, R. Wegerer, and M. Cardona, Coupling of Phonons to Crystal-Field Excitations in $NdBa_2Cu_3O_{7-\delta}$, Phys. Rev. Lett. **67**, 144 (1991).

[22] M. T. Hutchings, Point-charge calculations of energy levels of magnetic ions in crystalline electric fields, in *Solid State Physics*, Vol. 16, edited by Frederick Seitz and David Turnbull (Academic, New York, 1964), pp. 227–273.

[23] J. L. Prather, Atomic energy levels in crystals, Nat. Bur. Stand. (U.S.), Monogr. **19** (1961).

[24] A. J. Freeman and R. E. Watson, Theoretical investigation of some magnetic and spectroscopic properties of rare-earth ions, Phys. Rev. **127**, 2058 (1962).

[25] U. Walter, Treating crystal field parameters in lower than cubic symmetries, J. Phys. Chem. Solids **45**, 401 (1984).

[26] K. W. H. Stevens, Matrix elements and operator equivalents connected with the magnetic properties of rare earth ions, Proc. Phys. Soc. **65**, 209 (1952).

[27] A. J. Freeman and J. P. Desclaux, Dirac-fock studies of some electronic properties of rare-earth ions, J. Magn. Magn. Mater. **12**, 11 (1979).

[28] A. Bertin, Y. Chapuis, P. D. de Réotier, and A. Yaouanc, Crystal electric field in the $R_2Ti_2O_7$ pyrochlore compounds, J. Phys.: Condens. Matter **24**, 256003 (2012).

[29] K. R. Lea, M. J. M. Leask, and W. P. Wolf, The raising of angular momentum degeneracy of f-electron terms by cubic crystal fields, J. Phys. Chem. Solids **23**, 1381 (1962).

[30] G. E. Granroth, A. I. Kolesnikov, T. E. Sherline, J. P. Clancy, K. A. Ross, J. P. C. Ruff, B. D. Gaulin, and S. E. Nagler, SEQUOIA: A newly operating chopper spectrometer at the SNS, J. Phys.: Conf. Ser. **251**, 012058 (2010).

[31] G. L. Squires, *Introduction to Thermal Neutron Scattering* (Cambridge University Press, Cambridge, UK, 1978).

[32] J. Gaudet, A. M. Hallas, A. I. Kolesnikov, and B. D. Gaulin, Effect of chemical pressure on the crystal electric field states of erbium pyrochlore magnets, Phys. Rev. B **97**, 024415 (2018).

[33] B. Tomasello, C. Castelnovo, R. Moessner, and J. Quintanilla, Single-ion anisotropy and magnetic field response in the spin-ice materials $Ho_2Ti_2O_7$ and $Dy_2Ti_2O_7$, Phys. Rev. B **92**, 155120 (2015).

[34] A. J. Princep, H. C. Walker, D. T. Adroja, D. Prabhakaran, and A. T. Boothroyd, Crystal field states of Tb^{3+} in the pyrochlore spin liquid $Tb_2Ti_2O_7$ from neutron spectroscopy, Phys. Rev. B **91**, 224430 (2015).

[35] J. Gaudet, D. D. Maharaj, G. Sala, E. Kermarrec, K. A. Ross, H. A. Dabkowska, A. I. Kolesnikov, G. E. Granroth, and B. D. Gaulin, Neutron spectroscopic study of crystalline electric field excitations in stoichiometric and lightly stuffed $Yb_2Ti_2O_7$, Phys. Rev. B **92**, 134420 (2015).

[36] S. B. Lee, S. Onoda, and L. Balents, Generic quantum spin ice, Phys. Rev. B **86**, 104412 (2012).

[37] M. Ruminy, F. Groitl, T. Keller, and T. Fennell, Neutron Larmor diffraction investigation of the rare-earth pyrochlores $R_2Ti_2O_7$ (R = Tb, Dy, Ho), Phys. Rev. B **94**, 174406 (2016).

[38] S. W. Lovesey and U. Staub, Magnetoelastic model for the relaxation of lanthanide ions in $YBa_2Cu_3O_{7-\delta}$ observed by neutron scattering, Phys. Rev. B **61**, 9130 (2000).

[39] M. Ruminy, M. N. Valdez, B. Wehinger, A. Bosak, D. T. Adroja, U. Stuhr, K. Iida, K. Kamazawa, E. Pomjakushina, D. Prabakharan, M. K. Haas, L. Bovo, D. Sheptyakov, A. Cervellino, R. J. Cava, M. Kenzelmann, N. A. Spaldin, and T. Fennell, First-principles calculation and experimental investigation of lattice dynamics in the rare-earth pyrochlores $R_2Ti_2O_7$ (R = Tb,Dy,Ho), Phys. Rev. B **93**, 214308 (2016).

[40] M. Ruminy, S. Chi, S. Calder, and T. Fennell, Phonon-mediated spin-flipping mechanism in the spin ices $Dy_2Ti_2O_7$ and $Ho_2Ti_2O_7$, Phys. Rev. B **95**, 060414 (2017).

[41] R. Schedler, U. Witte, M. Loewenhaupt, and J. Kulda, Coupling between crystal field transitions and phonons in the $4f$-electron system $CeCu_2$, Phys. B (Amsterdam) **335**, 41 (2003).

[42] L. C. Chapon, E. A. Goremychkin, R. Osborn, B. D. Rainford, and S. Short, Magnetic and structural instabilities in $CePd_2Al_2$ and $LaPd_2Al_2$, Phys. B (Amsterdam) **378**, 819 (2006).

[43] D. T. Adroja, A. del Moral, C. de la Fuente, A. Fraile, E. A. Goremychkin, J. W. Taylor, A. D. Hillier, and F. Fernandez-Alonso, Vibron Quasibound State in the Noncentrosymmetric Tetragonal Heavy-Fermion Compound $CeCuAl_3$, Phys. Rev. Lett. **108**, 216402 (2012).

[44] T. Fennell, M. Kenzelmann, B. Roessli, H. Mutka, J. Ollivier, M. Ruminy, U. Stuhr, O. Zaharko, L. Bovo, A. Cervellino, M. K. Haas, and R. J. Cava, Magnetoelastic Excitations in the Pyrochlore Spin Liquid $Tb_2Ti_2O_7$, Phys. Rev. Lett. **112**, 017203 (2014).

[45] E. Constable, R. Ballou, J. Robert, C. Decorse, J.-B. Brubach, P. Roy, E. Lhotel, L. Del-Rey, V. Simonet, S. Petit, and S. deBrion, Double vibronic process in the quantum spin ice candidate $Tb_2Ti_2O_7$ revealed by terahertz spectroscopy, Phys. Rev. B **95**, 020415(R) (2017).

[46] R. A. Borzi, F. A. Gómez Albarracín, H. D. Rosales, G. L. Rossini, A. Steppke, D. Prabhakaran, A. P. Mackenzie, D. C. Cabra, and S. A. Grigera, Intermediate magnetization state and competing orders in $Dy_2Ti_2O_7$ and $Ho_2Ti_2O_7$, Nat. Commun. **7**, 12592 (2016).

[47] M. Orendáč, J. Hanko, E. Čižmár, A. Orendáčová, M. Shirai, and S. T. Bramwell, Magnetocaloric study of spin relaxation in dipolar spin ice $Dy_2Ti_2O_7$, Phys. Rev. B **75**, 104425 (2007).

[48] A. M. Hallas, J. Gaudet, M. N. Wilson, T. J. Munsie, A. A. Aczel, M. B. Stone, R. S. Freitas, A. M. Arevalo-Lopez, J. P. Attfield, M. Tachibana, C. R. Wiebe, G. M. Luke, and B. D. Gaulin,

XY antiferromagnetic ground state in the effective $S = 1/2$ pyrochlore $Yb_2Ge_2O_7$, Phys. Rev. B **93**, 104405 (2016).

[49] O. Arnold, J. C. Bilheux, J. M. Borreguero, A. Buts, S. I. Campbell, L. Chapon, M. Doucet, N. Draper, R. Ferraz Leal, M. A. Gigg, V. E. Lynch, A. Markvardsen, D. J. Mikkelson, R. L. Mikkelson, R. Miller, K. Palmen, P. Parker, G. Passos, T. G. Perring *et al.*, Mantid—Data analysis and visualization package for neutron scattering experiments, Nucl. Instrum. Methods Phys. Res. **764**, 156 (2014).

[50] R. T. Azuah, L. R. Kneller, Y. Qiu, C. M. Brown, J. R. D. Copley, R. M. Dimeo, and P. L. W. Tregenna-Piggott, DAVE: A comprehensive software suite for the reduction, visualization, and analysis of low energy neutron spectroscopic data, J. Res. Natl. Inst. Standards Technol. **114**, 341 (2009).